Turkish Journal of Electrical Engineering & Computer Sciences

http://journals.tubitak.gov.tr/elektrik/

Research Article

Turk J Elec Eng & Comp Sci
(2017) 25: 1827 – 1839

doi:10.3906/elk-1602-184

Optimal design of voltage regulators for static excitation system in synchronous generator to reduce shaft-induced voltage

Mahmoud SAMIEI MOGHADDAM*, **Mohammad TAVAKOLI BINA**,
Masoud ALIAKBAR GOLKAR, **Shokrollah SHOKRI KOJORI**
Faculty of Electrical Engineering, Khajeh Nasir Toosi University of Technology, Tehran, Iran

Received: 13.02.2016 • **Accepted/Published Online:** 27.06.2016 • **Final Version:** 29.05.2017

Abstract: Long-term shaft-induced voltage could harm synchronous generators, specifically their bearings and insulators. This paper investigates the reduction of shaft-induced voltage using both a passive filter and an active voltage regulator. An RLC circuit is used as a passive filter, and a DC-DC buck converter is used as an active voltage regulator. As a result, they remove high-frequency spikes, leading to the reduction of shaft-induced voltage. Buck converters show minimum-phase behavior and can pose as stable–casual converters. A 5 kW synchronous generator was considered for the laboratory setup in which a static excitation system using a 6-pulse thyristor rectifier supplies the rotor winding. Active and passive filters were placed between the rectifier and the excitation winding of the synchronous generator. Both simulations and experiments show that the suggested filters are capable of efficiently removing the parasitic capacitance, significantly mitigating shaft-induced voltage. However, the active voltage regulator performs better than the passive filter in reducing shaft-induced voltage. This reduction can increase the lifespan of bearings in a generator.

Key words: Bearing current, active voltage regulator, shaft-induced voltage, passive filter, static excitation system

1. Introduction

Shaft-induced voltage is a serious and unwanted issue related to synchronous generators. Shaft voltage is induced due to the transition of power electronic switches of the static excitation system, emitting electromagnetic interference that induces capacitive coupling voltage to the ground and, therefore, to the capacitive currents. Thus, these currents flow from the generator through the generator bearing to the ground.

There are four main effects of shaft-induced voltage in rotating machines; magnetic dissymmetry, axial shaft flux, external voltages applied to the rotor windings, and electrostatic charge [1]. Induced voltage caused by the rotor windings has been specified as a main reason for many unwanted problems such as leakage current, ball-bearing damage, and the reduction of a generator's lifespan.

In [2,3], an LC filter and a PWM inverter are proposed as a way to attenuate both common-mode and differential-mode voltages produced by the inverter. In [4,5], the authors investigate a passive LC-EMI filter designed to reduce bearing currents driven by a three-level inverter. In [6], the authors propose the use of a common-mode passive filter to reduce induced-shaft voltage and ground current issues of an induction motor that is supplied by a dual two-level inverter. A passive filter in [7,8] is suggested for a PWM inverter, which is made up of 2 small LC filters found between the inverter output and the motor. A hybrid EMI filter is presented in [9] in order to compensate for the common-mode voltage of PWM inverters. It consists of a single-

*Correspondence: samiei352@yahoo.com

leg four-level filter joined in series with a capacitor and a medium passive filter that attenuate high-frequency magnitude of the common-mode voltage. In [10], the authors focus on the development of VSI-output voltage as the driving source of bearing currents.

Significant research has been conducted to justify the shaft-induced voltage phenomenon and the related bearing current. A static excitation system is applied to a designed synchronous machine in [11]. Experiments on a 15-kW motor in [12,13] show that shaft-to-frame voltage varies up to 8 V due to the switching transitions of a voltage-source inverter; parasitic capacitances along with the high-frequency common-mode voltage of the PWM inverter are the sources of generating shaft-to-frame voltage.

A PWM method is presented in [14] for back-to-back AC-DC-AC converters in order to reduce common mode voltage of these converters. In [15], a methodology is proposed to identify the effect of the thickness of the insulating coat on leakage current reduction as a function of machine parameters. It is further proven that even by isolating one of the bearings a medium-voltage PWM inverter can still induce motor bearing currents. An analytical study in [16] describes a case related to the reciprocal effects on a wind generation system connected to a DC capacitive load, suggesting solutions to remedy the voltage issues encountered. In [17,18], systematic plans are presented to lower the common mode voltages of different converters, including the VSI and the CSI. Shami et al. address shaft end-to-end and shaft-to-frame voltages in [19]. An ungrounded common-mode equivalent circuit of the motor is examined in [20] in which the influence of further reduction via a new methodology is approved by determining shaft-induced voltage from the equivalent circuit and measurement of shaft-induced voltage. In [21], an experimental plan is proposed to develop a model of an AC machine in order to forecast leakage current and shaft-induced voltage. The effect of neutral voltages and end winding on shaft voltage is investigated in [22].

However, it is necessary to investigate the electrostatic analysis of the synchronous generator by studying the effect of parasitic capacitance on induced voltage. This paper presents a new model that considers all parasitic capacitances (up to 15 parasitic capacitances calculated by the finite-element method shown in Table 1) to calculate the shaft voltage in a synchronous generator when considering both passive filter and active voltage regulators. An active regulating method is also completely implemented using a buck converter to reduce the shaft-induced voltage produced by a 6-pulse thyristor rectifier. Since buck converters show minimum-phase behavior, they are stable and casual during various operating conditions. Therefore, this work concentrates on studying the external voltages supplied to the rotor windings as the other 3 mentioned sources of shaft voltage ([1]) are already discussed in the literature.

Table 1. Calculated parasitic capacitances.

Row	Mutual capacitance	Parasitic capacitance value [Pf]	Row	Mutual capacitance	Parasitic capacitance value [Pf]
1	C_{SW}	8207.3	9	C_{0SH}	332.68
2	C_{SR}	3480.7	10	C_{RW}	2449
3	C_{SSH}	2319.3	11	C_{RF}	1418.2
4	C_{SF}	1035.3	12	C_{RSH}	758.09
5	C_{0R}	333.26	13	C_{FW}	918.18
6	C_{0S}	367.74	14	C_{WSH}	2446.6
7	C_{0W}	352.33	15	C_{FSH}	1418.1
8	C_{0F}	273.51			

Switching components appear in the DC output voltage of excitation systems that are controlled by thyristors; therefore, capacitive coupling between the rotor windings and the shaft induces shaft voltages. The outline of the paper is as follows: first, parasitic capacitance is determined based on the finite element method MATLAB/SIMULINK is then used to simulate the static excitation system. Finally, the experiments conducted on a 5 kW synchronous generator are presented to verify the introduced analysis, modeling, and simulations.

2. Model representation

The structure of a synchronous generator can be seen in Figure 1. The figure also shows a cross section for the required model components, including that of the static excitation system. The following subsections explain the studies performed on the elements found in Figure 1.

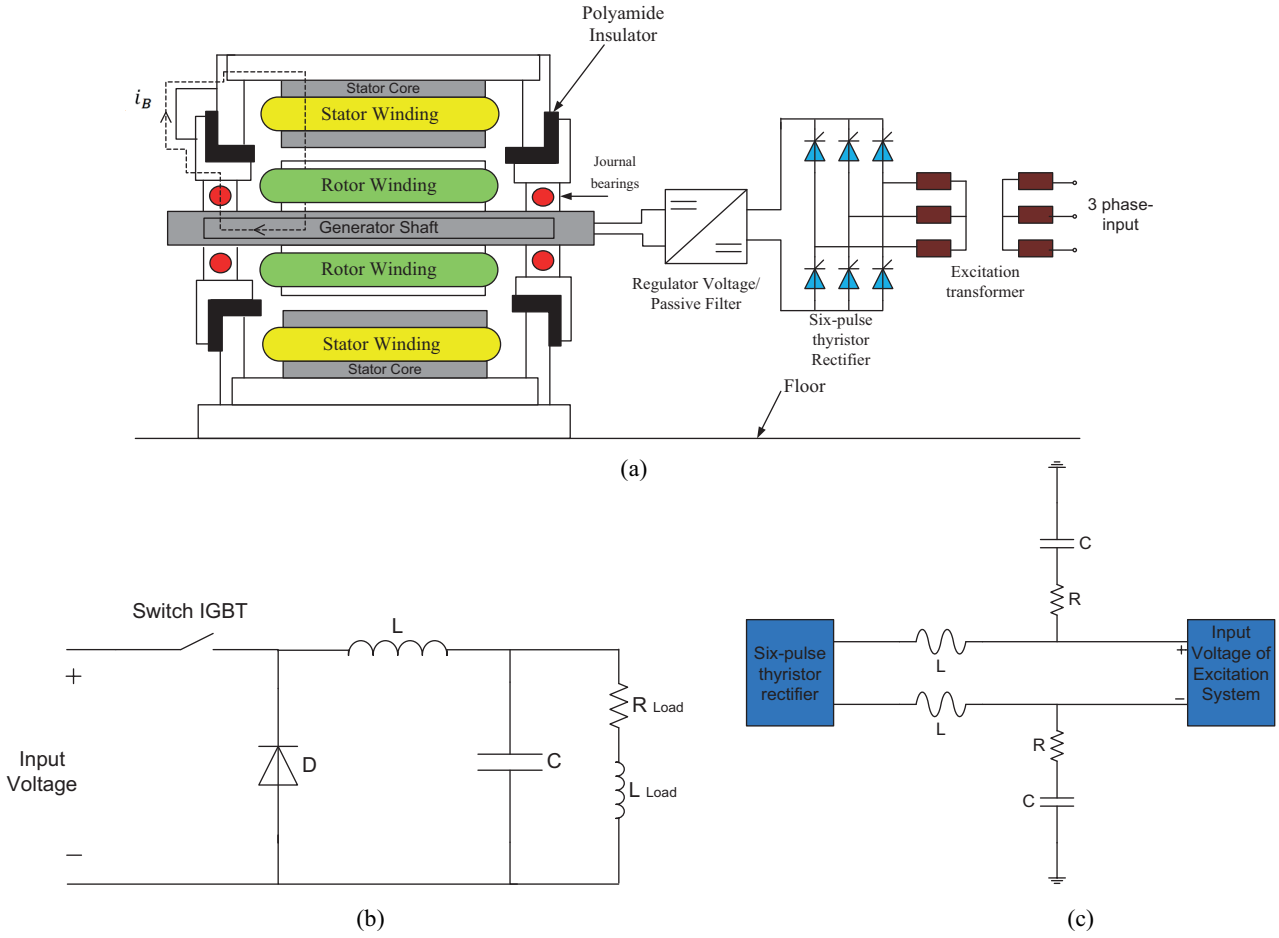

Figure 1. a) Comprehensive structure of the studied model, b) schematic of active regulator, and c) schematic of passive filter.

Figure 1a shows static excitation of a synchronous generator; the AC input 3-phase is first rectified by a thyristor bridge connected to DC voltage, which is then connected to the DC exciter with a passive filter. Figure 1b presents a RLC passive filter that is mathematically described in Section 2.3. An active regulator is shown in Figure 1c that is expressed mathematically in Section 2.2.

2.1. Parasitic capacitance calculation

Considering Figure 1a, 4 parasitic capacitances are derived in [23,24] between various parts of the synchronous generator as described below:

1) The bearing capacitance: The bearing capacitance is associated with the geometrical design of the bearing, load, speed, temperature, and characteristics of the lubricant.

$$C_b = \frac{N_b 4\pi\varepsilon_0\varepsilon_r}{(\frac{1}{R_b} - \frac{1}{R_b+R_c})} \tag{1}$$

where R_b is the radius of the ball, $R_b + R_c$ is the radius of the equivalent outer sphere, and N_b is the number of balls.

2) Stator winding to frame capacitance (C_{sf}) is calculated as

$$C_{sf} = \frac{K_{sf} N_s \varepsilon_r \varepsilon_0 (W_{d+} W_{s)} L_s}{d} \tag{2}$$

where N_s is the number of stator slots, and L_s, W_d, and W_s are the conductor length, depth, and width, respectively. A dielectric isolated the conductor and conduit by d meters with a permittivity of $\varepsilon_0\varepsilon_r$.

3) The stator to rotor coupling capacitance (C_{sr}) is given by

$$C_{sr} = \frac{K_{sr} N_r \varepsilon_0 W_r L_r}{g} \tag{3}$$

where C_{sr} consists of N_r sets of parallel conducting plates. The area of each plate is equal to the product of the length of the rotor (L_r) and the width of the rotor conductor near the rotor surface (W_r).

4) Rotor to frame capacitance (C_{rf}):

$$C_{rf} = \frac{K_{rf}\pi\varepsilon_0 L_r}{\ln(\frac{R_s}{R_r})} \tag{4}$$

where R_s is the inside radius of the outer cylinder (stator) and R_r is the outer radius of the inner cylinder (rotor). Parameter K is a scale factor applied to 2–4 above to enhance the fitted curve to the measured data. The required equations were collected from the textbook of engineering electromagnetic in [25]. The geometrical equations were taken from a reliance machine of varied frame size while the coefficient of K_{sf}, K_{sr}, and K_{rf} were calculated based on [26]. Figure 2 shows the capacitances system model in the observed synchronous generator.

The calculated parasitic capacitances are listed in Table 1. The subscript indices S, W, R, SH, F, and 0 show the stator, stator winding, rotor, shaft, field winding, and frame, respectively.

2.2. Active regulator parameters

Buck parameters are calculated based on the following equations [26]:

$$\frac{1}{\sqrt{LC}} << \omega_n \tag{5}$$

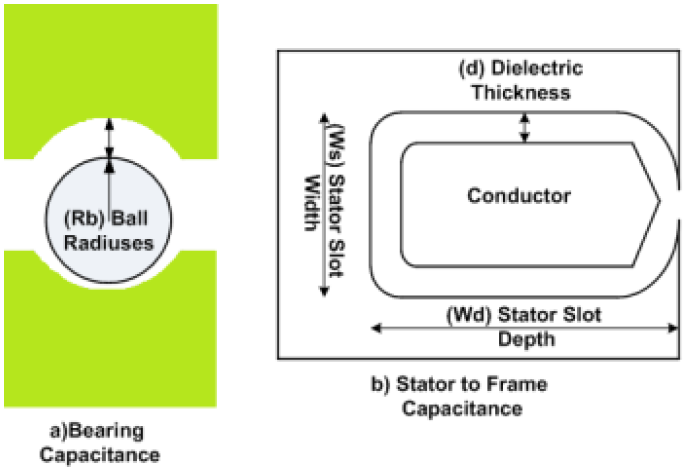

Figure 2. Representation of the capacitance system model in the studied synchronous generator.

$$\frac{1}{RC} << \frac{\omega_n}{Q} \tag{6}$$

ω_n can be calculated as follows:

$$\omega_n = \frac{\pi}{T_s}, \tag{7}$$

where T_s is the switching period:

$$\Delta V_0 = \frac{\Delta Q}{C} = \frac{1}{C}\frac{1}{2}\frac{\Delta I_L}{2}\frac{T_s}{2} \tag{8}$$

$$\Delta I_L = \frac{V_0}{L}(1-D)T_s \tag{9}$$

By replacing $.\Delta I_L$ from Eq. (9) with Eq. (8), the following is obtained:

$$\frac{\Delta V_0}{V_0} = \frac{1}{8}\frac{T_s^2(1-D)}{LC} = \frac{\pi^2}{2}(1-D)\left(\frac{f_c}{f_s}\right)^2, \tag{10}$$

where f_s is the switching frequency and f_c is the cut-off frequency, determined as

$$f_c = \frac{1}{2\pi\sqrt{LC}} \tag{11}$$

Eq. (10) shows that selecting an appropriate f_c efficiently lowers the voltage ripple. As a result, by converting the switching spike into ripples with small magnitude at the output of thyristor rectifier, the effect of parasitic capacitance can be decreased, which in turn results in reducing the shaft-induced voltage. A buck converter is chosen because of its minimum-phase behavior, introducing stable converters for this purpose.

2.3. Passive filter parameters

Power electronic devices serve as the most important resources of harmonic generation due to converter switching. Harmonic analysis plays an important role in control systems. Under transient conditions, such as short-

circuit or switching, current waveforms become distorted. Thus, applying passive filters is a conventional way to mitigate harmonic signals. These conventional methods could form a resonant circuit in parallel with load.

The parameters of a passive filter can be calculated as follows [6]:

$$\left.\begin{array}{l} X_L = L\omega_0 \\ X_C = \frac{1}{C\omega_0} \\ (n\omega_0)^2 = \frac{1}{LC} \end{array}\right\} \Rightarrow X_L = \frac{1}{n^2} X_C \tag{12}$$

$$Q_{ST} \frac{n.X_L}{R} \tag{13}$$

$$|I| = \frac{|V|}{\sqrt{R^2 + (X_c - X_L)^2}}, \tag{14}$$

where V is the applied voltage to the passive filter, I is the filter current, ω_0 is angular velocity at the main frequency, and ω_r is angular velocity at resonance frequency at the nth harmonic.

2.4. Simulation study

A schematic representation of the simulated system is shown in Figure 3, which demonstrates a 3-phase source applied to the system in which driving a motor is the prime mover of the synchronous generator. Additionally, a 6-pulse thyristor rectifier, followed by either an active regulator or a passive filter, provides the excitation system.

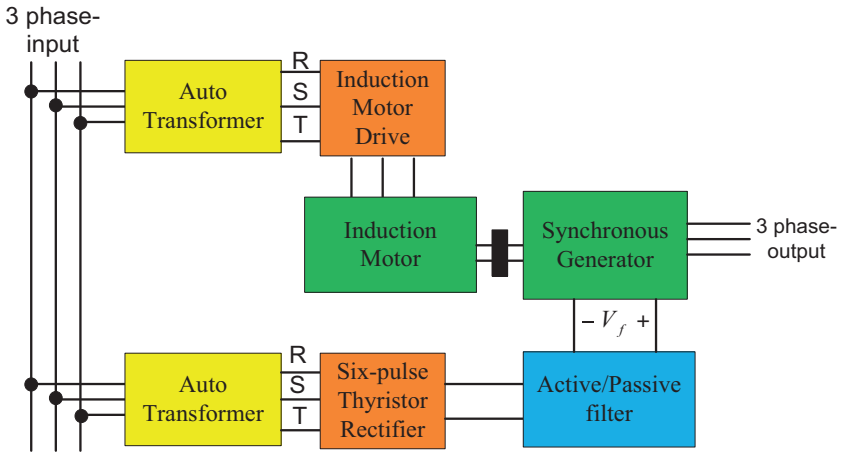

Figure 3. General schematic of the simulated system.

The generator exciter is actually fed by the DC voltage obtained from the passive filters' outcome. The filters attenuate high frequency spikes that are imposed by thyristor switching effects. The lower these high frequency components, the lower the amplitude of the shaft-induced voltage.

2.5. Parasitic capacitance identification

The finite element method (FEM) was used to calculate the parasitic capacitances introduced in the previous section. Maxwell employs the precise FEM to solve static, frequency-domain, and time-variant electromagnetic

and electric fields. To do so, the synchronous generator is divided into 6 separate parts (nodes) including the stator, stator winding, rotor, shaft, field winding, and frame. Figure 4 shows these parts corresponding to the electrical arrangement.

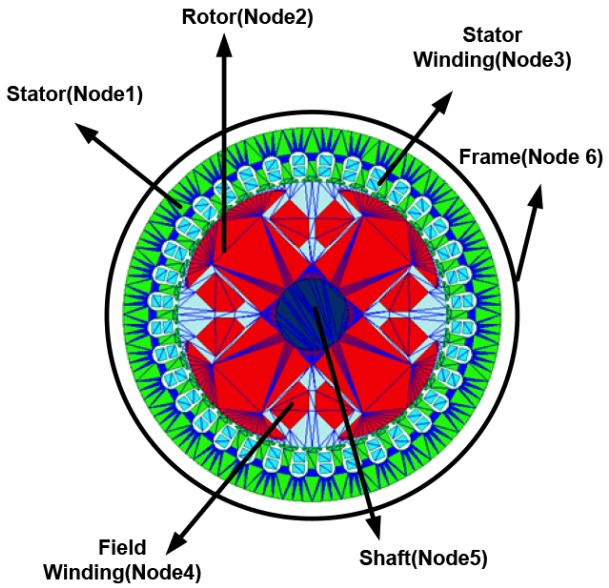

Figure 4. Six different parts (node) of the synchronous generator used to determine the parasitic capacitances.

Table 2 lists all symbols that are used to calculate capacitances in Table 1.

Table 2. List of symbols used to calculate capacitance.

Row	Symbol	Explanation
1	ε_0	permittivity of free space
2	ε_r	permittivity of lubricants
3	R_b	Ball Radiuses
4	R_c	Redial Clearance
5	N_b	number of balls
6	C_b	Bearing Capacitance
7	C_{sf}	Stator winding to frame capacitance
8	Ns	number of stator slot
9	L_s, W_d W_s	conductor meter long, deep and wide
10	d	dielectric isolated
11	K_{sf}	scale factor of Stator winding to frame
12	K_{sr}	scale factor of stator to rotor
13	N_r	sets of parallel conducting plates
14	W_rL_r	width and length of the rotor
15	g	Air Gap
16	K_{rf}	scale factor of Rotor to frame
17	R_s	inside radius of the outer stator
18	R_r	outer radius of the inner rotor

Maxwell calculates parasitic capacitance between 2 different conductors by simulating the electric field produced by the applied external voltage. The capacitance is then obtained by calculation of the energy stored

on the capacitor as follows:

$$C = \frac{2w_e}{v^2} \tag{15}$$

A regulator (either active or passive) is placed in between the 6-pulse thyristor-controlled rectifier and the excitation winding. In the case of the active regulator, a sliding-mode, nonlinear controller modulates the switch of the converter. It should also be noted that a PI controller was used to maintain the output voltage of the rectifier at a fixed value. The parameters of the buck converter are shown in Table 3.

Table 3. Parameters of the active regulator and passive filter.

Row		Parameter	Value
Active regulator	1	L (inductance)	430 μH
	2	R_L (inductance resistance)	20 $m\Omega$
	3	C (capacitor)	660 μF
	4	R_C (resistance of capacitor)	80 $m\Omega$
	5	R_t (resistance in the transistor)	20 $m\Omega$
	6	R_D (diode resistor)	16 $m\Omega$
	7	V_g (input voltage)	15 V
	8	V_o (output voltage)	30 V
	9	T_s (switching period)	20 μs
Passive filter	1	R (resistance)	70 $m\Omega$
	2	L (inductance)	560 μH
	3	C (capacitor)	470 μF

Figure 5 illustrates simulations of the described system, showing the total harmonic distortion (THD) for excitation voltage for an uncompensated case, passive filter, and active regulator. Simulations clearly show that including an active regulator significantly lowers the THD. This reduction in voltage ripples of excitation winding would decrease induced-shaft voltage in the synchronous generator because of the bypassing of parasitic capacitances.

As the high frequency spikes due to the rectifier switching decreases, the THD of the DC input voltage of excitation system decreases, leading to the reduction of induced-shaft voltage.

Figure 6 indicates the simulation results for voltage in phase "a" of the synchronous generator with and without regulators. The THD of voltage in phase "a" is 3.3% without a filter, while using a passive filter the THD decreases to 3.11%. In the case of an active regulator, the THD is 3.07%, the lowest among the three cases. Thus, the effect of parasitic capacitance on shaft-induced voltage of synchronous generator is reduced.

Simulations indicate that the active regulator is more effective than the passive filter in lowering the effects of parasitic capacitances.

3. Experimental confirmation

A general description of the experimental equipment is shown in Figure 7, consisting of a 3-phase autotransformer, a 5-kW induction motor with its corresponding AC drive, a 5-kW synchronous generator, a 6-pulse thyristor-controlled converter, and a compensator (either a passive or active regulator).

A 3-phase voltage (380 V line to line) is applied to an autotransformer, followed by a diode rectifier. After this, a 2-level inverter converts DC to AC using space vector modulation. Another autotransformer reduces the input voltage to be applied to the 6-pulse thyristor rectifier, in which the DC output voltage can be controlled by

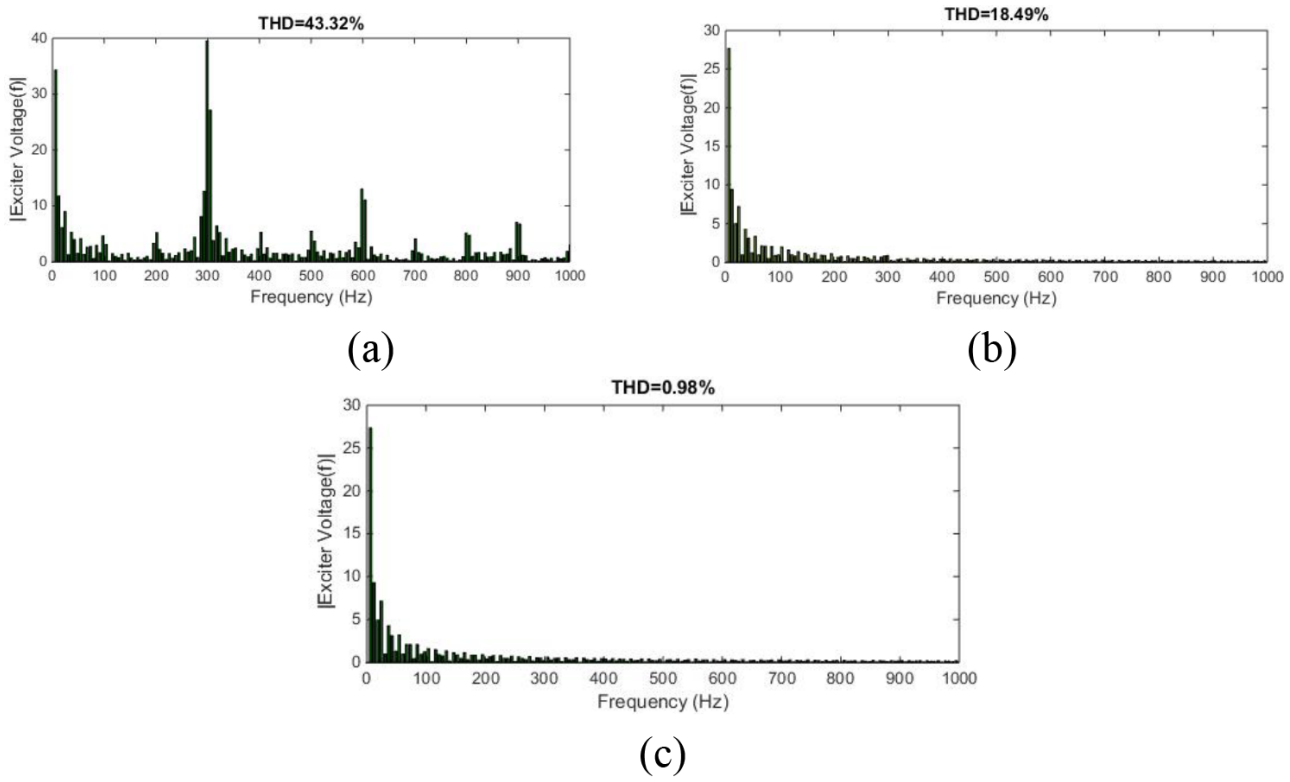

Figure 5. Simulated THD for excitation winding input voltage; a) excluding filter, b) including passive filter, c) including active regulator.

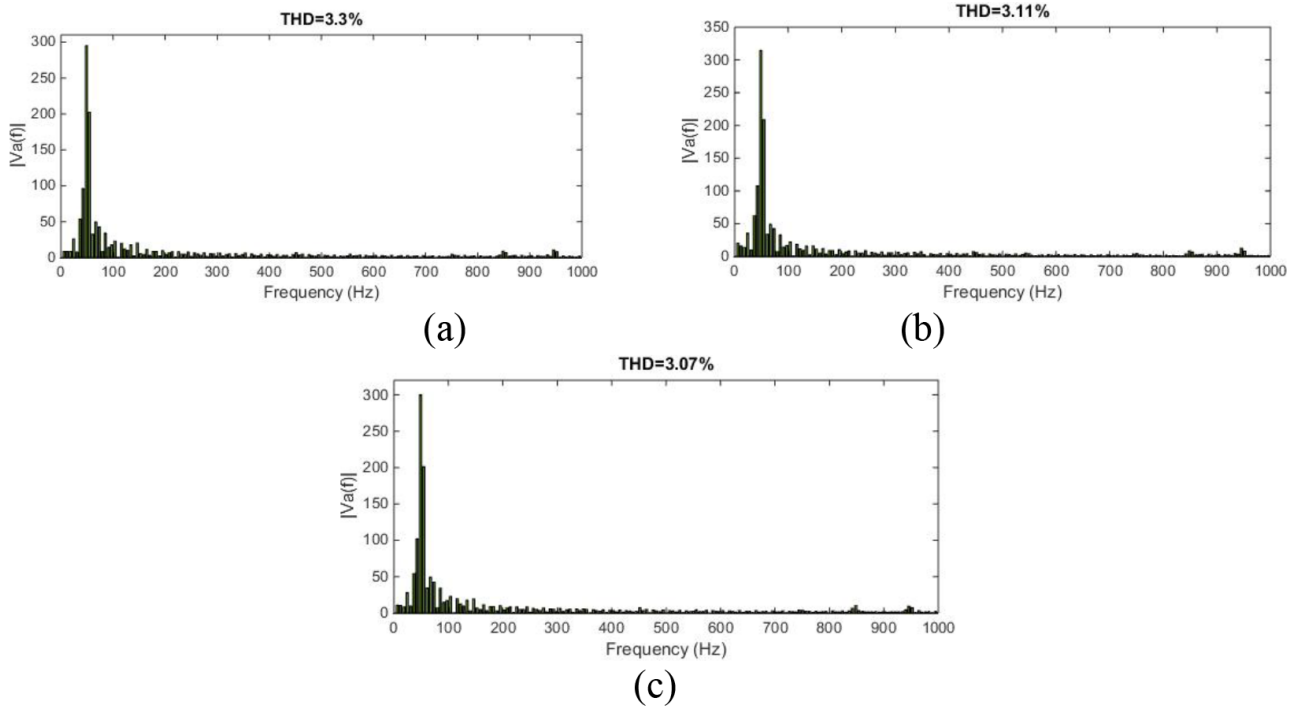

Figure 6. Simulation results of voltage in Phase A; a) excluding filter, b) with passive filter, c) with active regulator.

setting firing angle. The DC output voltage is then applied to the filter, which is then applied to the excitation winding. In order to measure the shaft voltage, it is necessary to insulate the bearings with respect to the stator case. Figure 8 shows how to insulate the generator bearings. After the insulation of bearings, the shaft-induced voltage will be measurable due to its parasitic capacitance.

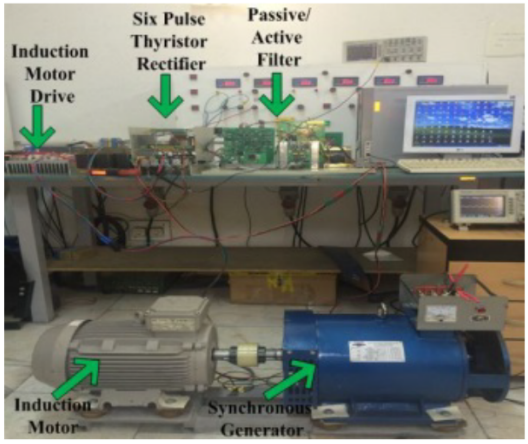

Figure 7. General description of the experimental equipment.

Figure 8. Insulation of synchronous generator bearings.

Figure 9 shows the experimental results for the THD of the excitation voltage with and without a compensator. Experiments show that using a regulator can cause the THD to be significantly reduced as previously verified by the simulation results. This reduction in voltage ripples of excitation winding would decrease induced-shaft voltage in the synchronous generator because of the bypassing of the parasitic capacitances.

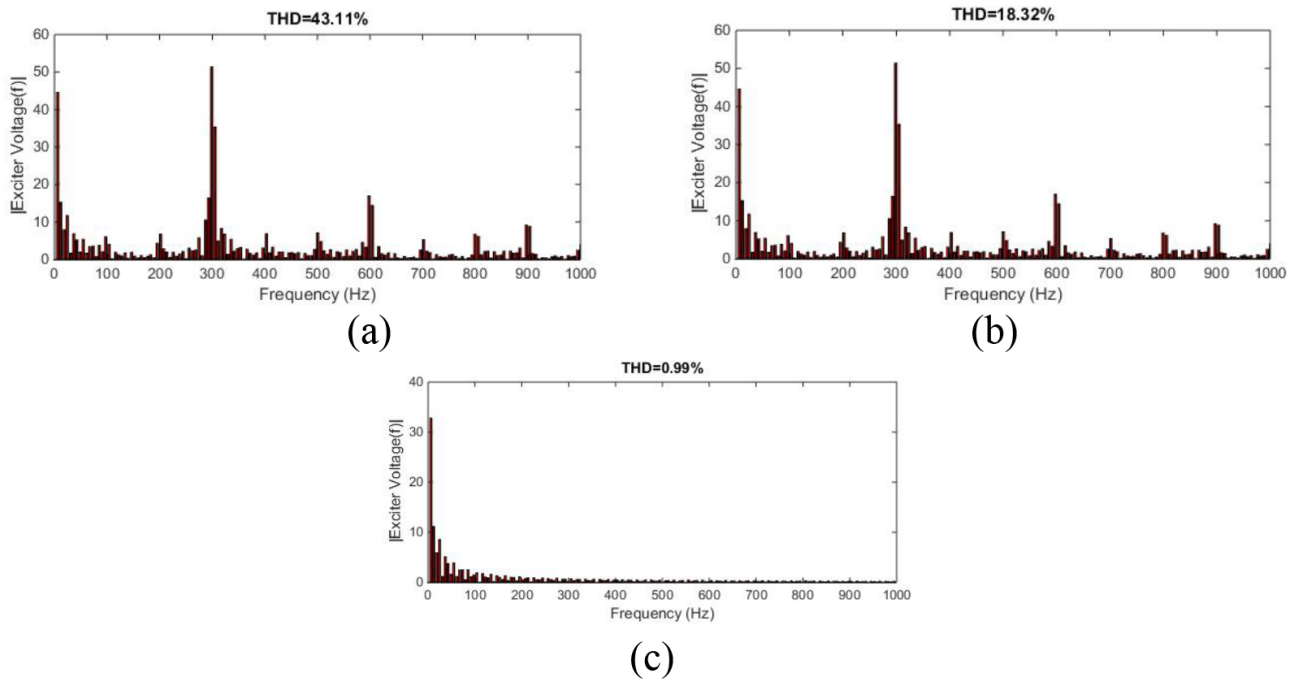

Figure 9. Experimental results of THD for excitation winding input voltage; a) excluding a filter, b) including passive filter, c) including active regulator.

Figure 10 indicates the experimental results of voltage in Phase A of the synchronous generator with and without a regulator. The THD of voltage in Phase A is decreased with the presence of both active regulator and passive filters, which means the reduction of high-frequency spikes on output voltage. Thus, the effect of parasitic capacitance on the shaft-induced voltage of the synchronous generator is reduced. These results were also verified by the simulations presented and discussed in the previous section.

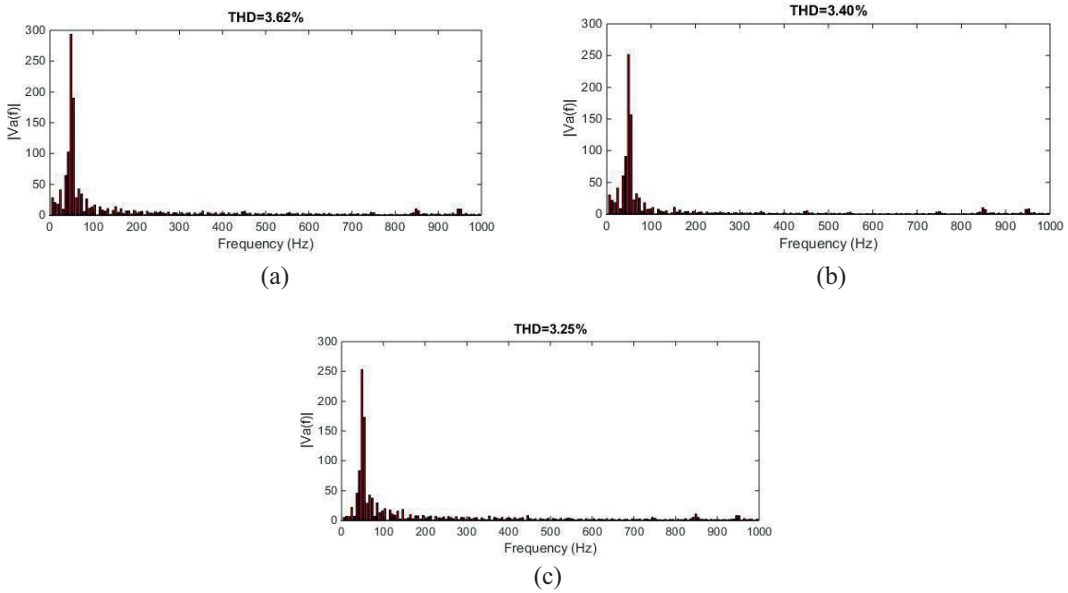

Figure 10. Experimental results of voltage in Phase A; a) excluding filter, b) with passive filter, c) with active regulator.

Shaft-induced voltage with respect to the ground is shown in Figure 11, with and without considering compensators.

As seen in Figure 11 and as shown in Table 4, the peak-to-peak of shaft voltage without a compensator is approximately 80.8 V and 58.4 V for the passive compensator and 40.8 V for the active regulator. This clearly shows that employing a compensator is an effective way to decrease shaft-induced voltage. Shaft voltage can cause the ionization of the bearing oil, reducing the effective lifespan of the bearing.

Table 4. Shaft voltage and THD comparison, excluding and including filters.

Parasitic capacitance	Excluding filter	Including passive filter	Including active regulator
Shaft voltage (peak–peak)	80.8	58.4	40.8
THD % (shaft voltage)	19.3%	11.41%	7.76%

It can be concluded that an active regulator reduces the magnitude of shaft-induced voltage more effectively. This is because of the better dynamic response of the active regulator, resulting in a significant reduction of shaft-induced voltage.

4. Conclusion

Various causes for shaft-induced voltage are reported in the literature. However, static excitation systems are the main source of shaft-induced voltage. An important task is the reduction of shaft voltage and bearing current to a harmless value in order to protect synchronous generators. This paper presents both a passive

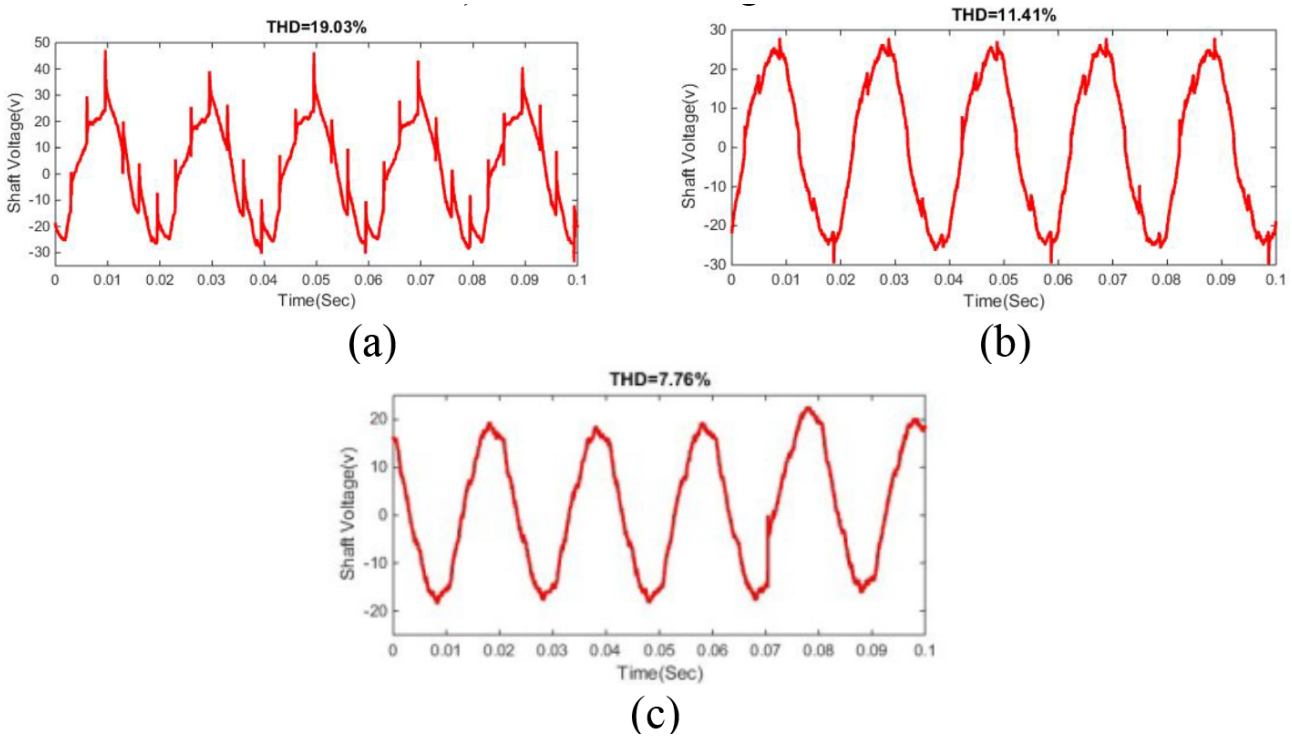

Figure 11. Experimental results of shaft-induced voltage; a) without filter, b) with passive filter, c) with active regulator.

filter and an active regulator for this purpose. A buck converter is used for an active regulator that shows minimum-phase behavior. Moreover, the FEM is used to work out 15 different parasitic capacitances for the proposed model. Both experimental and simulation results show that applying the suggested compensators is an effective way of controlling both shaft voltage and bearing currents in a synchronous generator. However, using an active rather than a passive regulator is a more effective way to reduce induced-shaft voltage.

References

[1] Golkhandan R, Bina MT, Golkar MA. A complete excitation-shaft-bearing model to overcome the shaft induced-voltage and bearing current. In: IEEE 2011 Power Electronics, Drive Systems and Technologies Conference; 16–17 February 2011; Tehran, Iran. New York, NY, USA: IEEE. pp. 362-366.

[2] Dianguo X, Qiang G, Wei W. Design of a passive filter to reduce common-mode and differential-mode voltage generated by voltage-source PWM inverter. In: IEEE 2006 Industrial Electronics; 6–10 November 2006; Paris, France. New York, NY, USA: IEEE. pp. 2483-2487.

[3] Qiang G, Dianguo X. A New approach to mitigate CM and DM voltage dv/dt value in PWM inverter drive motor systems. In: IEEE 2007 Applied Power Electronics Conference; 25 Feb–1 Mar 2007; Anaheim, CA, USA. New York, NY, USA: IEEE. pp. 1212-1216.

[4] Akagi H, Tamura S. A passive EMI filter for eliminating both bearing current and ground leakage current from an inverter-driven motor. IEEE T Power Electr 2006; 21: 1459-1469.

[5] Akagi H, Tamura S. A passive EMI filter for eliminating both bearing current and ground leakage current from an inverter-driven motor. In: IEEE 2005 Power Electronics Specialists Conference; 16 June 2005; Recife, Brazil. New York, NY, USA: IEEE. pp. 2442-2450.

[6] Kalaiselvi J, Srinivas S. Passive common mode filter for reducing shaft voltage, ground current, bearing current in dual two level inverter fed open end winding induction motor. In: IEEE 2014 Optimization of Electrical and Electronic Equipment; 22–24 May 2014; Bran, Romania. New York, NY, USA: IEEE. pp. 595-600.

[7] Pirouz HM, Bina MT, Kanzi K. A new approach to the modulation and DC-link balancing strategy of modular multilevel AC/AC converters. In: IEEE 2005 International Conference on Power Electronics and Drive Systems; 28 Nov–1 Dec 2005; Kuala Lumpur, Malaysia. New York, NY, USA: IEEE. pp. 1503-1507.

[8] Esmaeli A, Sun Y, Sun L. Mitigation of the adverse effects of PWM inverter through passive cancellation method. In: IEEE 2006 Systems and Control in Aerospace and Astronautics; 19–21 January 2006; Harbin, China. New York, NY, USA: IEEE. pp. 746-751.

[9] Vahedi H, Sheikholeslami A, Bina MT. Review and simulation of fixed and adaptive hysteresis current control considering switching losses and high-frequency harmonics. Advances in Power Electronics 2011; 11: 158-164.

[10] Pairodamo P, Suwanka S, Sangwong S. Design and implementation of a hybrid output EMI filter for high-frequency common-mode voltage compensation in PWM inverters. IEEE T Ind Appl 2009; 45: 1647-1659.

[11] Hyypio D. Mitigation of bearing electro-erosion of inverter-fed motors through passive common-mode voltage suppression. In: IEEE 2005 Industry Applications Conference; 12–16 October 2003; Piscataway, NJ, USA. New York, NY, USA: IEEE. pp. 576-583.

[12] Kumar Datta A, Dubey M, Jain S. Modelling and simulation of static excitation system in synchronous machine operation and investigation of shaft voltage. Advances in Electrical Engineering 2014; Article ID 727295, 9 pages, 2014. doi: 10.1155/2014/727295.

[13] Shami UT, Akagi H. Experimental discussions on a shaft end-to-end voltage appearing in an inverter-driven motor. IEEE T Power Electr 2009; 24: 1532-1540.

[14] Muetze A. On a new type of inverter-induced bearing current in large drives with oil-lubricated bearings. IEEE T Ind Appl 2010; 46: 240-248.

[15] Adabi ME, Vahedi A. A survey of shaft voltage reduction strategies for induction generators in wind energy applications. Renew Energ 2013; 50: 177-187.

[16] Rahmani B, Bina MT. Reciprocal effects of the distorted wind turbine source and the shunt active power filter: full compensation of unbalance and harmonics under 'capacitive non-linear load' condition. IET Power Electr; 6: 1668-682.

[17] Muetze A, Binder A. Calculation of influence of insulated bearings and insulated inner bearing seats on circulating bearing currents in machines of inverter-based drive systems. IEEE T Ind Appl 2006; 42: 965-972.

[18] Liu F, Zha X, Zhou Y, Duan S. Design and research on parameter of LCL filter in three-phase grid-connected inverter. In IEEE 2009 Power Electronics and Motion Control Conference; 7–20 May 2009; Wohan, China. New York, NY, USA: IEEE. pp. 2174-2177.

[19] Sanmin W, Zargari N, Bin W, Rizzo S. Comparison and mitigation of common mode voltage in power converter topologies. In IEEE 2004 Industry Applications Conference; 3–7 October 2004; Toronto, Canada. New York, NY, USA: IEEE. pp. 1852-1857.

[20] Shami UT, Akagi H. Identification and discussion of the origin of a shaft end-to-end voltage in an inverter-driven motor. IEEE T Power Elect 2010; 25: 1615-1625.

[21] Isomura Y, Yamamoto K, Morimoto S, Maetani T Watanabe, Nakano K. Study of the further reduction of shaft voltage of brushless DC motor with insulated rotor driven by PWM inverter. In IEEE 2013 Power Electronics and Drive Systems; 22–25 April 2013; Kitakyushu, Japan. New York, NY, USA: IEEE. pp. 1184-1189.

[22] Zare F. Practical approach to model electric motors for electromagnetic interference and shaft voltage analysis. IET Electr Power App 2010; 4: 727-738.

[23] Adabi J, Zare F, Ghosh A. End-winding effect on shaft voltage in AC generators. In IEEE 2009 Power Electronics and Applications European Conference; 8–10 September 2009; Barcelona, Spain. New York, NY, USA: IEEE. pp. 965-972.

[24] Busse D, Erdman J, Kerkman RJ, Schlegel D. Skibinski G. System electrical parameters and their effects on bearing currents. IEEE T Ind Appl 2002; 33: 577-584.

[25] Hayt WH. Engineering Electromagnetics. 5th ed. New York, NY, USA: McGraw-Hill, 1989.

[26] Rashid MH. Power Electronics Handbook. 2nd ed. New York, NY, USA: Academic Press, 1998.